techniques and later transient techniques (potential or current step) should be applied. Until now very little has been known about the mechanism and kinetics of these processes, and we wish to pursue experimental studies in this direction.

During the discharging (hydrogen oxidation) cycle surface oxidation may take place if the final potential is much more positive than the hydrogen equilibrium potential (or metal corrosion potential). In such cases the surface oxidation current should be taken into account. In order to avoid such oxidation, discharging at a constant potential, at which there is no surface oxidation, may be carried out.

In the treatment of the hydrogen evolution reaction, the Langmuir isotherm for the adsorbed hydrogen was assumed. The use of Frumkin or Temkin isotherms would only change slopes of $\Theta$ *vs.* logarithm of time and, consequently, $X_0$ *vs.* log $t$.

The DAE method has proven to be stable and fast (less than 1 min per simulation), and it may be used to solve other diffusion-kinetic equations in electrochemistry, with the assumed precision, even in the presence of fast reaction kinetics.

## Acknowledgments

Financial support from NSERC and FCAR (grant for D.G.) is gratefully appreciated. Dr. B. Sommeÿer from Centrum voor Wiskunde en Informatica, Stichting Mathematisch Centrum, Amsterdam, is acknowledged for suggesting use of the DAE method.

Manuscript submitted Dec. 12, 1994; revised manuscript received April 27, 1995.

*Université de Sherbrooke assisted in meeting the publication costs of this article.*

REFERENCES

1. B. E. Conway and J. Wojtowicz, *J. Electroanal. Chem.*, **326,** 277 (1992).
2. Q. M. Yang, M. Ciureanu, D. H. Ryan, and J. O. Ström-Olsen, *This Journal,* **141,** 2108 (1994).
3. Q. M. Yang, M. Ciureanu, D. H. Ryan, and J. O. Ström-Olsen, *ibid.*, **141,** 2113 (1994).
4. A. Lasia, *Int. J. Hydrogen Energy,* **18,** 557 (1993).
5. A. Lasia, in *Current Topics in Electrochemistry,* **2,** 239 (1994).
6. A. Lasia and A. Rami, *J. Electroanal. Chem.,* **294,** 123 (1990).
7. D. A. Harrington and B. E. Conway, *ibid.*, **221,** 1 (1987).
8. D. Britz, *Digital Simulations in Electrochemistry,* Springer-Verlag, Berlin (1988).
9. K. E. Brenan, S. L. Campbell, and L. R. Petzold, *Numerical Solution of Initial-Value Problems in Differential-Algebraic Equations,* Elsevier, New York (1989).
10. L. Bai, *J. Electroanal. Chem.,* **355,** 37 (1993).

# *In Situ* X-Ray Absorption Studies of a Pt-Ru Electrocatalyst

**James McBreen* and Sanjeev Mukerjee***

*Department of Applied Science, Brookhaven National Laboratory, Upton, New York 11973, USA*

ABSTRACT

X-ray absorption studies (XAS) were done on a carbon supported Pt-Ru electrocatalyst in 1 *M* $HClO_4$. Results at the Pt $L_3$ and $L_2$ edges confirmed that the Pt was alloyed with Ru and that the Ru content was about 25 atomic percent. There was a large excess of unalloyed Ru, with only about 10% of the Ru alloyed with the Pt. The Pt XAS indicated that the Ru increased the Pt d band vacancies and decreased the Pt-Pt bond distances from 2.77 Å to values between 2.71 and 2.73 Å. The bifunctional mechanism for methanol oxidation on Pt-Ru electrocatalysts needs to be modified to account for the effect of these electronic changes on the adsorption of H and CO residues from methanol decomposition. There are significant changes in the Pt XAS in going from the reversible hydrogen potential to 0.24 V. This may be due to the onset of the formation of RuOH species on the alloy. Further fine tuning of the electronic structure and the electrocatalysis may be possible through the use of ternary alloys.

## Introduction

The high activity of Pt-Ru electrocatalysts for methanol oxidation has been known for thirty years.[1,2] The early work on these catalysts, particularly at Shell Research Limited, has been reviewed by McNicol.[3,4] Léger and Lamy have reviewed work done during the eighties.[5] There has recently been a resurgence of activity in the area.[6-14] A comparative study of the activity of various Pt binary alloys for methanol oxidation, published in 1992, indicates that Pt-Ru is still the best catalyst.[15] Ross, in a review, stressed the need to apply modern characterization techniques, including x-ray absorption spectroscopy (XAS), to complex catalysts such as Pt-Ru.[16] Since then he and his co-workers have made considerable progress in characterizing well-defined planar polycrystalline Pt-Ru electrodes and have been able to correlate surface structure with activity.[6-9] There is a recent review of this work.[17] So far there is no report on the application of XAS to Pt-Ru electrocatalysts.

Recently we have completed *in situ* XAS studies, in 1 *M* $HClO_4$, on a series of carbon supported binary Pt alloy electrocatalysts, where Pt was alloyed with first row transition metals (Cr, Mn, Fe, Co, and Ni).[18,19] The effect of the alloying element on the Pt d band occupancy was determined by analyzing the Pt $L_3$ and $L_2$ x-ray absorption near edge fine structure (XANES), following the methods of Mansour and his co-workers.[20-22] The effect of the alloying element on the Pt-Pt bond distance could be derived from an analysis of the Pt $L_3$ extended x-ray absorption fine structure (EXAFS). Evidence for corrosion or any redox process involving the alloying element could be derived from the K edge XANES of the first row transition metal. This paper reports a similar investigation on a carbon supported Pt-Ru electrocatalyst.

## Experimental

*Electrodes and cell.*—The carbon supported Pt-Ru catalyst was obtained from Johnson-Matthey, Inc., West Deptford, NJ. The powder was fabricated into an electrode wafer using standard fuel cell electrode fabrication techniques. The electrode composition, by weight, was 76% carbon supported catalyst, 12% carbon fibers, and 12% PTFE (Teflon T-30). The catalyst, carbon fibers, and the Teflon T-30 were dispersed ultrasonically in water. The PTFE was coagulated by the addition of 1 ml of 0.1 *M* $CF_3SO_3H$, and the material was cast into a sheet on a vacuum table paper making apparatus. The sheet (21 $cm^2$) was dried at 80°C in air and sintered under argon at 320°C for 5 min. The sheet weighed 0.8 g and was 0.6 mm thick. Elec-

* Electrochemical Society Active Member.

trode disks (19 mm diam) were punched from the sheet, soaked overnight in 1 *M* $HClO_4$, and were incorporated into a spectroelectrochemical cell with an uncatalysed PTFE-bonded carbon counterelectrode and a Nafion 117 (Du Pont) separator. Apart from separating the working and counterelectrodes, the main function of the separator was the prevention transport of evolved gases from the counterelectrode to the working electrode. Each gasket in the spectroelectrochemical cell was sized 0.025 mm thinner than the corresponding component. This maintained all components under compression and prevented complications in the spectra due to random density fluctuations caused by gas bubbles. The working and counterelectrodes were flooded with 1 *M* $HClO_4$. Provisions were made for an SCE reference electrode with a Nafion tube salt bridge that was sheathed in a PTFE tube. Other details of the spectrochemical cell are published elsewhere.[23]

*XAS measurements.*—The electrochemistry of the cell was checked by doing several sweeps (usually three) at 0.1 mV/s in the potential envelope of 0.0 to 0.7 V *vs.* a reversible hydrogen electrode. On the final sweep the electrode was held at 0.0 V and an XAS scan was done in an energy range that covered both the Pt $L_3$ and $L_2$ edges. Measurements were also taken at 0.24 and 0.54 V. The electrode was swept again to 0.0 V and XAS scans were made at the Ru K edge at 0.0, 0.24, 0.54, and 0.84 V. This covers the complete potential range normally encountered in methanol oxidation.

XAS measurements were made at Beam Line X11A at NSLS with the storage ring operating at 2.52 GeV and a current between 110 and 250 mA. The monochromator was operated in the two-crystal mode using Si(111) crystals. The monochromator was detuned by 15% to reject higher harmonics. In the case of both Pt and Ru the experiments were done in the transmission mode with three detectors. The third detector was used in conjunction with a reference sample, which was a Pt foil in the case of Pt and an Ru black/BN sample for Ru. The respective lengths of the incident ($I_o$), transmission ($I_t$), and reference ($I_r$) ionization chambers were 6, 12, and 6 in. For the Pt measurements the $I_o$ chamber was filled with $N_2$ and the other two with Ar. For Ru all chambers were filled with Ar. A slit height of 1.0 mm was used in the Pt measurements. For Ru it was 0.5 mm. Because of the low absorption of the other cell components at these high energies, and the uniformity of the electrode, the data quality was excellent.

*Data analysis.*—The methods used in analyzing the Pt XANES data and determination of the Pt d band vacancies followed those of Mansour and co-workers[20-22] and are described in detail elsewhere.[18,19] The EXAFS data were analyzed by methods described in detail in previous publications.[18,19,24] Phase and amplitude data for Pt-Pt interactions were derived from Pt foil data at liquid nitrogen temperature and from the FEFF program of Rehr.[25] The FEFF program was also used to derive phase and amplitude parameters for Pt-Ru, Ru-Pt, Ru-Ru, and Ru-O interactions. In the EXAFS analysis correlation effects between the coordination number ($N$) and the Debye-Waller factor ($\Delta\sigma^2$) and between the bond distance ($R$) and the potential shift ($\Delta E_o$) were checked by comparing $k^1$ and $k^3$ weighted fits.[26] The fitting was done by an iterative process till the same parameters gave good fits with both weightings.

## Results and Discussion

*XAS.*—Analysis of the XAS showed that the respective edge jumps at the Pt $L_3$ edge were 0.11 and 0.09. This indicated that the respective Ru and Pt loadings were 1.63 mg/cm$^2$ and 0.90 mg/cm$^2$ for a total loading of 2.53 mg/cm$^2$. This gives an atomic ratio of Ru to Pt of 3.43:1.

*Pt XANES.*—Figures 1 and 2 shows the Pt XANES at 0.0, 0.24, and 0.54 V at the respective Pt $L_3$ and $L_2$ edges. The Pt $L_3$ XANES for Pt foil and carbon supported Pt in 1 *M* $HClO_4$, at 0.54 V, are identical.[18] This indicates that alloying with Ru causes electronic effects on the Pt. The results in Fig. 1 indicate that at 0.0 V the white line at the Pt $L_3$ edge

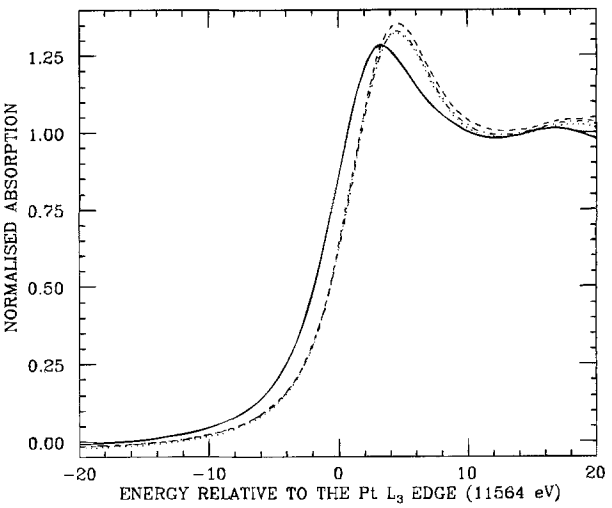


**Fig. 1. Pt $L_3$ XANES, Pt foil (——), Pt-Ru at 0.0 V (– – –), 0.24 V (---), and 0.54 V (····).**

is slightly higher and wider than at the other two potentials. However, the changes at 0.0 V as compared to 0.54 V are much less for the Pt-Ru alloy than for a pure Pt on carbon (Pt/C) catalyst[18]. With Pt/C there is no increase in the peak height at 0.0 V. However, there is considerable widening of the Pt $L_3$ white line on the high energy side of the peak. This widening of the white line has been observed by Mansour and co-workers[20-22] and by Boudart and co-workers[27] on oxide-supported catalysts in a hydrogen atmosphere in the gas phase. Thus the widening of the white line cannot be attributed to other electrochemical effects such as anion or water adsorption. Boudart attributed this to the transition of electrons into unoccupied Pt-H antibonding orbitals.[27] This could indicate surface segregation of Ru in the alloy or reduction in hydrogen adsorption on Pt. Ross [6] has actually found surface segregation of Pt in bulk alloys so the latter explanation is more plausible. The results suggest that alloying with Ru affects and most likely reduces the adsorption of hydrogen on platinum.

Table I shows the calculated Pt d band vacancies for the three potentials. In the double-layer region (0.54 V) the d band vacancies are similar to those obtained for Pt-Ni alloys (0.409) [18,19] and are greater than those found for Pt-Fe alloys (0.368). This compares with a value of 0.329 for a Pt/C catalyst. So alloying with Ru causes an increase in the number of Pt d band vacancies.

*Pt EXAFS.*—Figure 3 shows the Pt EXAFS at 0.54 V and Fig. 4 shows the Fourier transform. The parameters used for

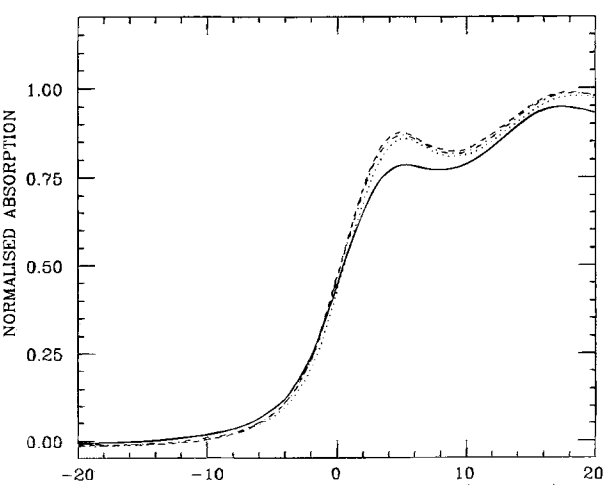


**Fig. 2. Pt $L_2$ XANES, Pt foil (——), Pt-Ru at 0.0 V (– – –), 0.24 V (---), and 0.54 V (····).**

**Table I. Results of Pt XANES analysis.**

| Electrode potential (V) | Pt d band vacancy per atom |
|---|---|
| 0.00 | 0.462 |
| 0.24 | 0.423 |
| 0.54 | 0.397 |

the forward and inverse transforms are given in Table II. Figure 5 shows a Pt-Pt and Pt-Ru two shell fit of the inverse transform in k space. Figures 6 and 7 show the corresponding real and imaginary fits in r space. Even though there were beats in the EXAFS, all the spectra at the Pt $L_3$ edge could be easily fitted with two shell fits, with physically reasonable parameters. There was no evidence for a Pt-O contribution, even in $k^1$ weighted transforms. For these two shell fits the error limits are ±15% for N and ±0.01 Å for R. [18]

The coordination number data indicate that the ratio of Pt to Ru varies between 10:3 and 8:3. If this is the case, then only about 10% of the Ru present is alloyed with Pt. This result is rather surprising but subsequent analysis of the Ru EXAFS supports this. Table III gives the results of the Pt EXAFS analysis at the various potentials. The results at 0.0 V differed in that the Pt-Pt bond length was slightly shorter and the Pt coordination number was somewhat higher. This was checked by doing the analysis over different $\Delta k$ ranges with various $k$ weightings. In EXAFS analysis bond distances can be determined with much more precision than coordination numbers. The fact that the Pt-Pt bond distances change is a strong indication of restructuring of the Pt-Ru particles in going from 0.24 to 0.0 V. Recent EXAFS results on carbon supported Pt shows an increase in the magnitude of the first Pt-Pt peak in the Fourier transform at 0.0 V. [28] In this case there is no change in the Pt-Pt bond distances. Data analysis, with checks for correlation effects, indicate an increase in the Pt-Pt coordination number at negative potentials.[29] This may be due to restructuring of the Pt surface. A similar mechanism may occur here. Reduction of Ru species on the alloy could also contribute to surface restructuring at negative potentials. This would be consistent with the increase in the Pt d band vacancies at 0.0 V. The total first shell coordination (Pt + Ru) is 10 at 0.24 V and 12 at 0.0 V. For Pt on carbon the first shell Pt-Pt coordination is 8 at 0.54 V and 10 at 0.0 V. This indicates a particle size of ~35 Å, [18,30] whereas the total coordination of the first shell of the Pt-Ru alloy indicated a particle size of ~50 Å. This is similar to that found when Pt is alloyed with first row transition metal elements.[18] The increased particle size is due to the thermal processing in making the alloy catalyst.[19] In our work on other binary Pt alloys we found that there is an inverse relationship between the Pt-Pt bond length and the number of Pt d band

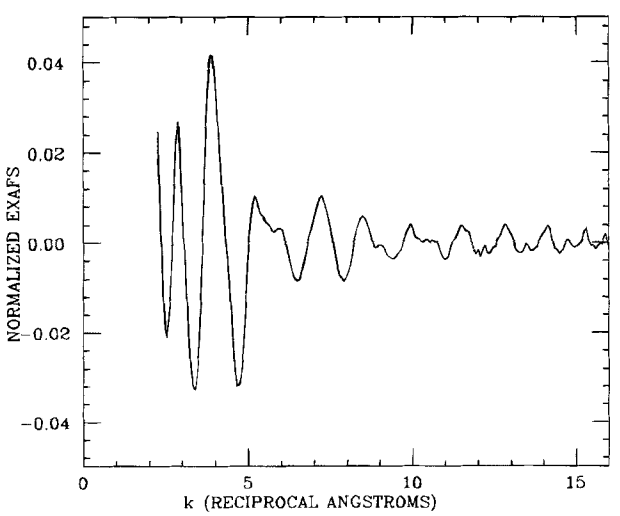


**Fig. 3. Pt EXAFS for Pt-Ru at 0.54 V.**

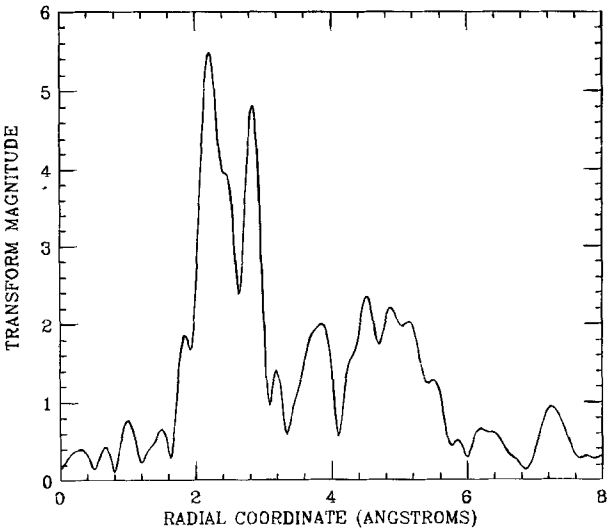


**Fig. 4. Fourier transform of data in Fig. 3, $k^3$ weighted, $\Delta k$ = 2.8 to 13.1 Å$^{-1}$.**

vacancies.[18] Thus for Pt-Ru the XANES and EXAFS results are consistent in that at 0.0 V there is an increase in the d band vacancies and a concomitant contraction in the Pt-Pt bond length. The results here are very similar to those found for Pt alloyed with first row transition elements in that alloying with Ru decreases the Pt-Pt bond distance.

*Ru XANES.*—Figure 8 shows Ru XANES for the electrocatalysts at various potentials. XANES at these high energies are of limited value in detecting redox processes because the edge shift with increasing oxidation state is small. Nevertheless, some changes can be observed at 0.84 V. This is undoubtedly due to the formation of species in a higher oxidation state and dissolution of the Ru. Dissolution of Ru is known to occur at potentials more positive to 0.7 V. [6]

*Ru EXAFS.*—Figure 9 shows the Ru EXAFS at 0.0 V, and Fig. 10 shows the effect of potential on the Fourier transform. There is an Ru-O contribution at 1.5 Å that changes significantly at 0.84 V. Analysis of the Ru EXAFS was difficult. Estimates of the Ru-O contribution were obtained by doing $k^3$ weighted transforms, back transforming the Ru-O contribution ($\Delta r$ = 0 to 1.75 Å), and doing a single-shell fit. The use of a $k^3$ weighted transform yields better separation of the Ru-O contribution and facilitated estimation of the Ru-O parameters. The results could be fitted to an Ru-O bond length of 2.02 Å at 0.0 V and 1.94 Å at 0.84 V. The bond length was 1.96 Å at the other two potentials. After many iterations, it was found that the spectra at 0.84 V could be best fitted to a two-shell Ru-Ru and Ru-O fit by fixing the Ru-O bond distance at 1.94 Å. This gave an Ru-O coordination number of ~3. At the other potentials the data could be easily fitted to a similar two-shell fit by fixing the Ru-O bond distance to the values given above. However, unlike the data at 0.84 V, the data could be fitted to a wide range of Ru-O coordination numbers. This is probably due to the weaker Ru-O bond at negative potentials. The data were simply fitted by fixing the O coordination number at three. The parameters used in doing the data analysis are given in Table IV and Table V gives the results. Figures 11 shows a

**Table II. Fourier transform parameters used in analyzing Pt EXAFS.**

| Electrode potential (V) | $k^n$ | $\Delta k$ (Å$^{-1}$) | $\Delta r$ (Å) |
|---|---|---|---|
| 0.00 | 3 | 2.8 to 13.1 | 1.44 to 3.16 |
| 0.24 | 3 | 2.8 to 15.0 | 1.40 to 3.4 |
| 0.54 | 3 | 2.73 to 14.8 | 1.38 to 3.2 |

$k^n$: weighting for Fourier transform.
$\Delta k$: integration range in k space for Fourier transform.
$\Delta r$: range for inverse transform.

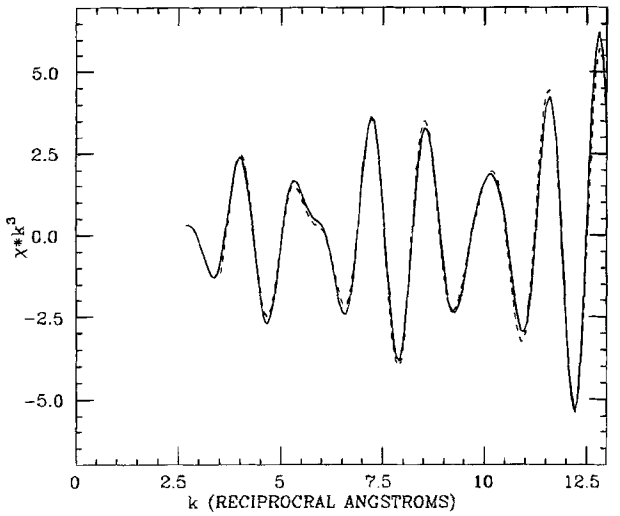


**Fig. 5. A two-shell fit for the inverse transform of the Fourier transform of Pt EXAFS at 0.54 V in k space, $k^3$ weighted, data (——), fit (– – –).**

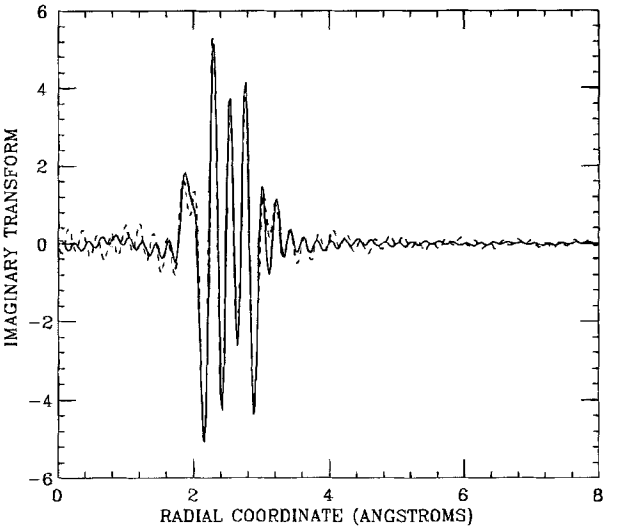


**Fig. 7. Fits for the imaginary part of the Fourier transform of data in Fig. 5 in r space, $k^1$ weighted, $\Delta k$ = 3 to 14 Å$^{-1}$, data (——), fit (– – –).**

typical fit for the data in $k$ space. The fact that the data could be fitted without including an Ru-Pt contribution further supports the fact that only a small fraction (~10%) of the Ru is alloyed with Pt. The main conclusion that can be drawn from the Ru EXAFS is that the $RuO_x$ undergoes at least one redox process in the potential range for methanol oxidation. This can be seen in the changes in the Ru-O bond length. The contraction in the bond length at more positive potentials is also consistent with the decrease in the Debye-Waller factor at positive potentials. At positive potentials the increase in the Ru-O peak in Fig. 10 and the decrease in the Ru-Ru peak indicates oxidation of the Ru. Unfortunately, no conclusions can be drawn about the Ru in the alloy. Detailed XAS studies, at the Ru K edge, are needed on Pt-Ru alloy catalysts with no excess unalloyed Ru.

*Mechanism of methanol oxidation.*—The bifunctional mechanism for the catalysis of Pt-Ru was first presented by Watanabe and Motoo.[31] According to the mechanism Pt sites catalyze the dehydrogenation of methanol and the oxidation of the hydrogen atoms. On pure Pt the reaction is "poisoned" because of absorption of the CO residues from methanol decomposition. On Pt-Ru adsorbed oxygen-containing species on the Ru facilitate oxidative removal of the CO residues. This mechanism has successfully explained many aspects of the catalysis including the different optimum Pt:Ru surface atom ratios for methanol and CO oxidation.[6,7] However, recent work by Vielstich and co-workers[11,32] indicates that the bifunctional mechanism needs to be modified to account for electronic effects of the Ru on the Pt. FTIR studies show a higher frequency for the CO stretch on Pt-Ru, implying a lower energy of absorption for CO on the alloy.[31] More recent results show that the peak potential for the CO residue formation is shifted 70 mV in the negative direction on the alloy.[11] An additional catalytic effect due to electronic interactions in the alloy has to be involved. The present work indicates that Ru has electronic effects on the Pt. There is no evidence in the present work that alloying promotes OH absorption on the Pt. In the previous work on alloys of first row transition metals[18,19] it was found that OH absorption was inhibited and no OH absorption could be observed even at 0.84 V. The same is likely to be true here and Ru is necessary to provide the oxygen-containing species for oxidation of the CO residues. Electronic effects on alloying can explain the lower energy of CO absorption.[32] The present work also indicates that alloying with Ru also affects the adsorption of H on Pt. Reduction of the hydrogen absorption and the provision of Pt sites could account for the negative shift in the potential for the formation of absorbed CO. Adzic *et al.* have proposed that reduced adsorption of H can have further electrocatalytic effects on the oxidation of small organic molecules.[33] The Pt EXAFS results indicate that changes occur in the alloy on going from 0.0 to 0.24 V. These changes are most likely due to the formation of RuOH and a relaxation of the Pt-Ru bonding. The formation of RuOH represents the "turn on" of the electrocatalytic effect. The present work and the results of Vielstich[11,31] indicate that it is necessary to modify the bifunctional mechanism and include electronic effects.

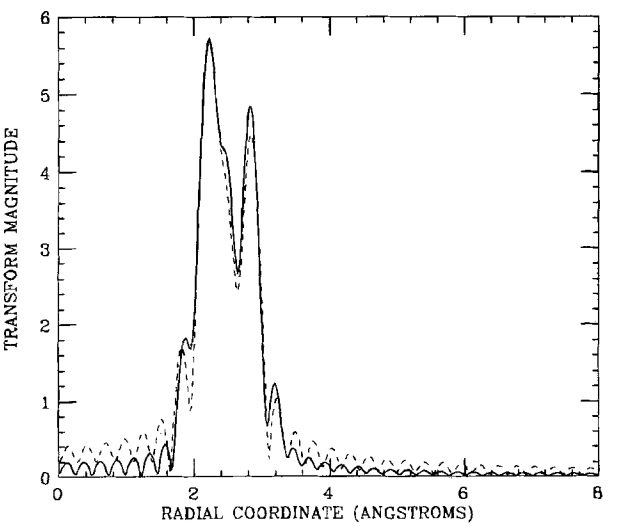


**Fig. 6. Fits for the real part of the Fourier transform of data in Fig. 5 in r space, $k^3$ weighted, $\Delta k$ = 3 to 14 Å$^{-1}$, data (——), fit (– – –).**

**Table III. Fitting parameters for the Pt EXAFS for the Pt-Ru catalyst at various potentials.**

| Electrode potential (V) | Shell | Calculated parameters | | | |
|---|---|---|---|---|---|
| | | $N$ | $R$ (Å) | $\Delta\sigma^2$ (Å$^2$) | $\Delta E_o$ (eV) |
| 0.00 | Pt-Pt | 9.64 | 2.71 | 0.007 | 1.93 |
| | Pt-Ru | 2.71 | 2.67 | 0.0029 | −6.61 |
| 0.24 | Pt-Pt | 7.03 | 2.73 | 0.0049 | 0.63 |
| | Pt-Ru | 2.95 | 2.67 | 0.0019 | −7.07 |
| 0.54 | Pt-Pt | 7.39 | 2.72 | 0.005 | 3.64 |
| | Pt-Ru | 2.57 | 2.68 | 0.001 | −6.75 |

$N$: coordination number.
$R$: coordination distance.
$\Delta\sigma^2$: Debye-Waller factor.
$\Delta E_o$: inner potential shift.

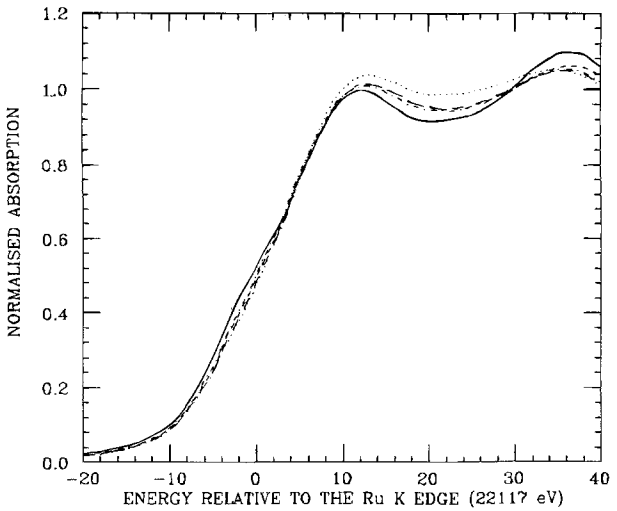


**Fig. 8. Ru K edge XANES, Ru black (——), Pt-Ru at 0.0 V (– – –), 0.24 V (---), 0.54 V (-- -- --), and 0.84 V (····).**

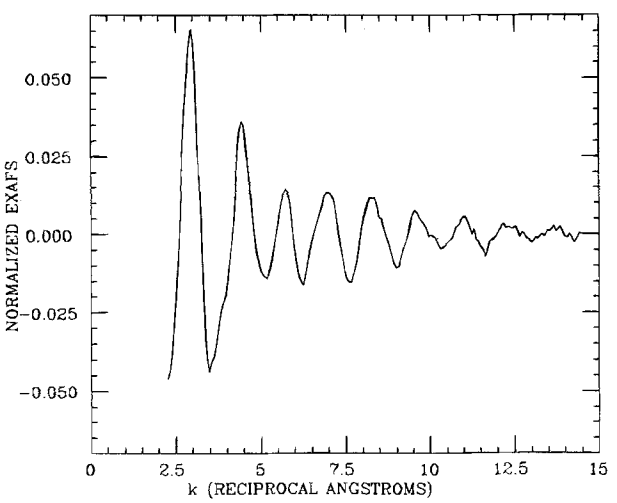


**Fig. 9. Ru K edge EXAFS Pt-Ru at 0.0 V.**

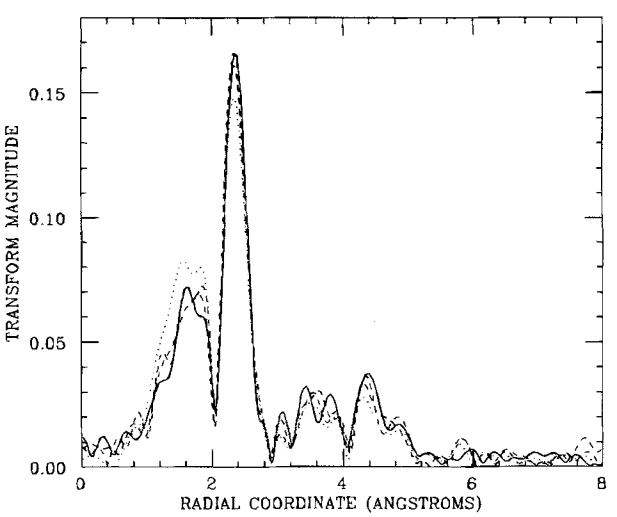


**Fig. 10. Fourier transform of Ru EXAFS, Pt-Ru at 0.0 V (——), 0.24 V (– – –), 0.54 V (---), and 0.84 V (····), $k^1$ weighted, $\Delta k$ = 2.6 to 13 Å$^{-1}$.**

## Conclusions

XAS studies at the Pt $L_3$ and $L_2$ edges show that the Pt is alloyed with Ru and that the Ru modifies the electronic structure of the Pt. The bifunctional mechanism for the electrocatalysis of methanol oxidation needs to be modified to take into account the effect of the increase in Pt d band vacancies on the adsorption of H and CO residues. This result indicates that further improvements in electrocatalytic activity may be achieved through further modifications in the electronic structure by the use of ternary alloys. The XAS results at the Ru K edge are less conclusive because of a large excess of unalloyed Ru in the electrocatalyst.

**Table IV. Parameters used in analyzing Ru EXAFS.**

| Electrode potential (V) | $k^n$ | $\Delta$k (Å$^{-1}$) | $\Delta$r (Å) |
|---|---|---|---|
| 0.00 | 3 | 2.61 to 13.9 | 0 to 3.22 |
| 0.24 | 3 | 2.62 to 12.64 | 0 to 3.08 |
| 0.54 | 3 | 2.61 to 12.71 | 0 to 3.2 |
| 0.84 | 3 | 2.55 to 12.8 | 0 to 3.22 |

**Table V. Fitting parameters for Ru EXAFS. Numbers in brackets were fixed as discussed in the text.**

| Electrode potential (V) | Shell | Calculated parameters | | | |
|---|---|---|---|---|---|
| | | $N$ | $R$ (Å) | $\Delta\sigma^2$ (Å$^2$) | $\Delta E_o$ (eV) |
| 0.00 | Ru-Ru | 5.75 | 2.66 | 0.0041 | 3.90 |
| | Ru-O | (3.00) | (2.02) | 0.033 | −0.96 |
| 0.24 | Ru-Ru | 6.14 | 2.66 | 0.0049 | 4.32 |
| | Ru-O | (3.00) | (1.96) | 0.029 | 6.34 |
| 0.54 | Ru-Ru | 5.74 | 2.66 | 0.051 | 4.66 |
| | Ru-O | (3.00) | (1.96) | 0.028 | 5.63 |
| 0.84 | Ru-Ru | 5.61 | 2.66 | 0.0048 | 4.53 |
| | Ru-O | 3.18 | (1.95) | 0.016 | 6.74 |

## Acknowledgments

This work was supported by the Assistant Secretary for Energy Efficiency and Renewable Energy, Office of Transportation Technologies, Electric and Hybrid Propulsion Division, USDOE under Contract Number DE-AC02-76CH00016.

The authors gratefully acknowledge support of the U.S. Department of Energy, Division of Materials Sciences, under Contract Number DE-FG05-89ER45384 for its role in development and operation of Beam Line X-11 at the National Synchrotron Light Source (NSLS). The NSLS is supported by the Department of Energy, Division of Materials Sciences under Contract Number DE-AC02-76CH00016.

Manuscript submitted Jan. 24, 1995; revised manuscript received May 26, 1995.

*Brookhaven National Laboratory assisted in meeting the publication costs of this article.*

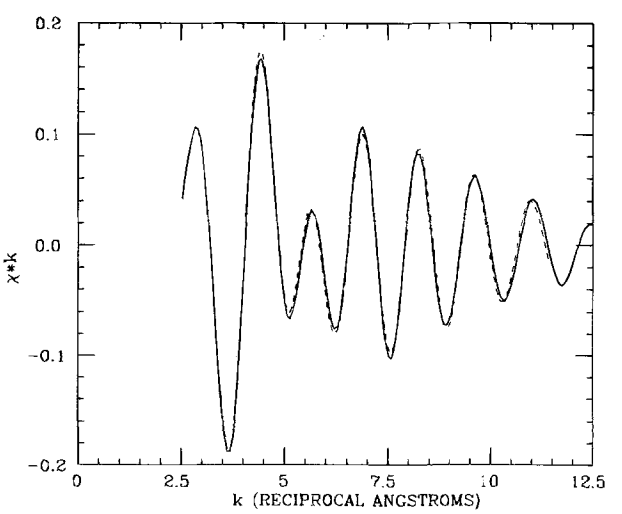


**Fig. 11. Fit in k space of inverse of Fourier transform of Ru EXAFS for Pt-Ru at 0.84 V, $k^1$ weighted, data (——), fit (– – –).**

REFERENCES

1. J. O'M. Bockris and H. Wroblowa, *J. Electroanal. Chem.*, **7,** 428 (1964).
2. O. A. Petry, B. I. Podlovchenko, A. N. Frumkin, and H. Lal, *ibid.*, **10,** 253 (1965).
3. B. D. McNicol, *ibid.*, **118,** 71 (1981).
4. B. D. McNicol, in *Power Sources for Electric Vehicles,* B. D. McNicol and D. A. J. Rand, Editors, pp. 807-838, Elsevier, Amsterdam (1984).
5. J.-M. Léger and C. Lamy, *Ber. Bunsenges. Phys. Chem.*, **94,** 1021 (1990).
6. H. A. Gasteiger, N. Marković, P. N. Ross, Jr., and E. J. Cairns, *J. Phys. Chem.*, **97,** 12020 (1993).
7. H. A. Gasteiger, N. Marković, P. N. Ross, Jr., and E. J. Cairns, *ibid.*, **98,** 617 (1994).
8. H. A. Gasteiger, N. Marković, P. N. Ross, Jr., and E. J. Cairns, *This Journal,* **141,** 1795 (1994).
9. H. A. Gasteiger, N. Marković, P. N. Ross, Jr., and E. J. Cairns, *Electrochim. Acta,* **39,** 1825 (1994).
10. T. Iwasita, R. Dalbeck, E. Pastor, and X. Xia, *ibid.*, **39,** 1817 (1994).
11. M. Krausa and W. Vielstich, *J. Electroanal. Chem.*, **379,** 307 (1994).
12. R. Ianniello, V. M. Schmidt, U. Stimming, J. Stumper, and A. Wallau, *Electrochim. Acta,* **39,** 1863 (1994).
13. G. Méli, J.-M. Léger, C. Lamy, and R. Durand, *J. Appl. Electrochem.*, **23,** 197 (1993).
14. C. Lamy and J.-M. Léger, *J. Phys.*, **4,** C1-253 (1994).
15. D. S. Cameron, G. A. Hards, and D. Thomsett, *Proc. Workshop on Direct Methanol-Air Fuel Cells,* A. R. Landgrebe, R. K. Sen, and D. J. Wheeler, Editors, PV 92-14, pp. 10-23, The Electrochemical Society, Proceedings Series, Pennington, NJ (1992).
16. P. N. Ross, Jr., *Electrochim. Acta,* **36,** 2053 (1991).
17. P. N. Ross, Jr., and H. A. Gasteiger, *Int. J. of Hydrogen Energy,* In press.
18. S. Mukerjee, S. Srinivasan, M. P. Soriaga, and J. McBreen, *This Journal,* **142,** 1409 (1995).
19. S. Mukerjee, S. Srinivasan, M. P. Soriaga, and J. McBreen, *J. Phys. Chem.*, **99,** 4577 (1995).
20. A. N. Mansour, Ph.D. Thesis, North Carolina State University, Raleigh, NC (1983).
21. A. N. Mansour, J. W. Cook, Jr., D. E. Sayers, R. J. Emrich, and J. R. Katzer, *J. Catal.*, **89,** 464 (1984).
22. A. N. Mansour, J. W. Cook, Jr., and D. E. Sayers, *J. Chem. Phys.*, **28,** 2330 (1984).
23. J. McBreen, W. E. O'Grady, K. I. Pandya, R. W. Hoffman, and D. E. Sayers, *Langmuir,* **3,** 428 (1987).
24. K. I. Pandya, W. E. O'Grady, D. A. Corrigan, J. McBreen, and R. W. Hoffman, *J. Phys. Chem.*, **94,** 21 (1990).
25. J. J. Rehr, J. Mustre de Leon, S. I. Zabinsky, and R. C. Albers, *J. Am. Chem. Soc.*, **113,** 5135 (1991).
26. D. C. Koningsberger, in *Synchrotron Techniques in Interfacial Electrochemistry,* C. A. Melandres and A. Tadjeddine, Editors, pp. 181-198, Kluwer Academic Publishers, Dorddrecht (1994).
27. M. G. Samant and M. Boudart, *J. Phys. Chem.*, **95,** 4070 (1991).
28. P. G. Allen, S. D. Conradson, M. S. Wilson, S. Gottesfeld, I. D. Raistrick, J. Valerio, and M. Lovato, *Electrochim. Acta,* **39,** 2415 (1994).
29. S. Mukerjee and J. McBreen, *This Journal,* Submitted.
30. R. B. Greegor and F. W. Lytle, *J. Catal.*, **63,** 476 (1980).
31. M. Watanabe and S. Motoo, *J. Electroanal. Chem.*, **60,** 275 (1975).
32. T. Iwazita, F. C. Nart, and W. Vielstich, *Ber. Bunsenges. Phys. Chem.*, **94,** 1030 (1990).
33. R. R. Adzic, A. V. Tripkovic, and W. E. O'Grady, *Nature,* **296,** 137 (1982).

# Temperature Effect on the Electrocrystallization Processes of Gold in Ammoniacal Medium

**Gabriel Trejo**

*Centro de Investigación y Desarrollo Tecnológico en Electroquímica CIDETEQ, Parque Tecnológico Sanfandila, Pedro Escobedo, Qro. Apdo. 064 C.P. 76700, Mexico*

**Adrián F. Gil* and Ignacio González****

*Departamento de Química, Area de Electroquímica, Universidad Autónoma Metropolitana-Iztapalapa 09340, A.P. 55-534 México D.F.*

ABSTRACT

Gold electrodeposition has been studied on glassy carbon from Au(I) ammoniacal solution. The current transients obtained from potential step perturbations show a typical metallic nucleation growth controlled by diffusion; this process is influenced by adsorption of the different chemical species on the surface. Diffusion coefficients were calculated for Au(I) at different temperatures. It was also found that the increase in the temperature provokes the modification of the nucleation mechanism.

## Introduction

The electrodeposition and electrowinning of gold are normally performed using cyanide-based baths. However, these baths have the great disadvantage of being strong pollutants because the cyanide ion is among the products obtained. For this reason, alternative nonpollutant baths have been researched (*e.g.*, those based on thiourea, thiosulfate, and ammonia). Unfortunately there are few works on this matter (*e.g.*, work of Rausepp and Allgood on the gold-thiourea complex[1]); on the other hand, the ammonia bath has been studied for leaching and electrodeposition of noble metals, *e.g.*, silver,[2] and good results have been reported by Meng for gold leaching.[3] However, a study on the thermodynamics and electrochemical behavior for Au(III) reduction in this medium has not been reported to our knowledge. Because the ammonia bath seems to be a good alternative for these processes, this bath has been selected in this work as a first choice.

To investigate the influence of the temperature on gold electrodeposition, voltammetric and potentiostatic studies were undertaken. When the experimental results were compared with the corresponding theoretical models, it was found that the temperature has great influence on the system studied, since it provokes a change in the nucleation process at high temperatures.

* Electrochemical Society Student Member.
** Electrochemical Society Active Member.